Catalyzed Gasoline Particulate Filters Reduce Secondary Organic Aerosol Production from Gasoline Direct Injection Vehicles

Patrick Roth,[†,‡] Jiacheng Yang,[†,‡] Emmanuel Fofie,[†,‡] David R. Cocker, III,[†,‡] Thomas D. Durbin,[†,‡] Rasto Brezny,[§] Michael Geller,[§] Akua Asa-Awuku,*[,†,‡,∥] and Georgios Karavalakis*[,†,‡]

[†]University of California, Bourns College of Engineering, Center for Environmental Research and Technology (CE-CERT), 1084 Columbia Avenue, Riverside, California 92507, United States

[‡]Department of Chemical and Environmental Engineering, Bourns College of Engineering, University of California, Riverside, California 92521, United States

[§]Manufacturers of Emission Controls Association, 2200 Wilson Boulevard, Suite 310, Arlington, Virginia 22201, United States

[∥]Department of Chemical and Biomolecular Engineering, A. James Clark School of Engineering, University of Maryland, College Park, Maryland 20742, United States

S *Supporting Information*
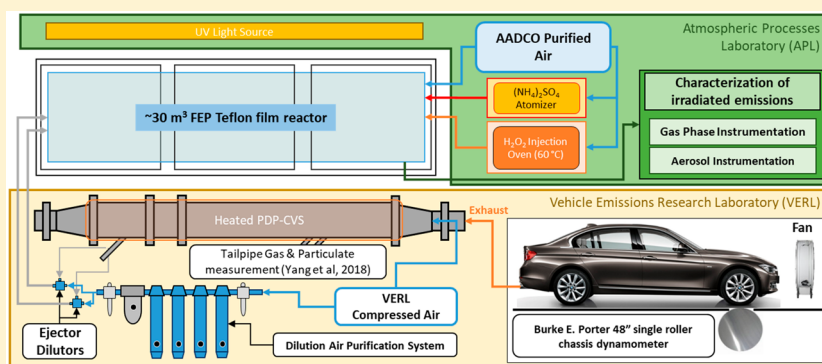
ABSTRACT: The effects of photochemical aging on exhaust emissions from two light-duty vehicles with gasoline direct injection (GDI) engines equipped with and without catalyzed gasoline particle filters (GPFs) were investigated using a mobile environmental chamber. Both vehicles with and without the GPFs were exercised over the LA92 drive cycle using a chassis dynamometer. Diluted exhaust emissions from the entire LA92 cycle were introduced to the mobile chamber and subsequently photochemically reacted. It was found that the addition of catalyzed GPFs will significantly reduce tailpipe particulate emissions and also provide benefits in gaseous emissions, including nonmethane hydrocarbons (NMHC). Tailpipe emissions composition showed important changes with the use of GPFs by practically eliminating black carbon and increasing the fractional contribution of organic mass. Production of secondary organic aerosol (SOA) was reduced with GPF addition, but was also dependent on engine design which determined the amount of SOA precursors at the tailpipe. Our findings indicate that SOA production from GDI vehicles will be reduced with the application of catalyzed GPFs through the mitigation of reactive hydrocarbon precursors.

■ INTRODUCTION

Mobile sources are major contributors of emissions, especially in urban areas.[1] On-road vehicles equipped with internal combustion engines are known to emit nitrogen oxides (NO_x), carbon monoxide (CO), particulate matter (PM), and volatile organic compounds (VOCs).[2] While vehicular NO_x, CO, and VOC emissions have been reducing over the past years as a result of tightening regulations imposed by environmental and governmental agencies,[3,4] several urban and rural areas across the United States and especially in California are characterized as nonattainment for air pollutant emissions.[5] Directly emitted PM from the vehicle's exhaust is comprised by a complex mixture of constituents, including sulfate, metals, and black

carbon, as well as primary organic aerosol (POA).[6] Studies have shown that PM emissions can be deposited deep into the lungs, inducing oxidative stress and respiratory diseases.[7,8] Other studies have shown that PM emissions influence the cardiovascular system.[9]

Emissions of NO_x, VOCs, and other semivolatile compounds are responsible for the formation of secondary organic aerosol (SOA) through the photo-oxidation of these species in

the atmosphere.[10,11] Emissions of NO_x and VOCs can undergo atmospheric reactions resulting in the formation of secondary lower volatility organic gases. As the gases continue to react, their volatility decrease until these gases nucleate (to form new particles) or condense onto existing particles and ultimately increase the atmospheric organic aerosol (OA) mass (the organic fraction of particles). The mechanism for the formation of SOA from anthropogenic or biogenic sources is not entirely clear as it involves complex processes, with the number of organic compounds participating in SOA formation being unknown.[12,13] Studies have reported that SOA accounts for the largest fraction of atmospheric OA, accounting for approximately 30−90% of total OA in megacities.[12,14,15] Recent studies have shown that gasoline vehicles, a major source of VOC emissions, dominate the production of SOA in urban areas compared to diesel vehicles, at least in the United States.[16] This phenomenon can be confirmed by the fact that gasoline vehicle sales far exceed those of diesel vehicles in the U.S. compared to the European Union, and also by the fact that gasoline fuel consists of lighter and more volatile hydrocarbons in the range of $C_4−C_{10}$, which are major SOA precursors.[11,17]

The significant contribution of gasoline vehicles to the SOA budget has been shown in several studies.[18−20] Gordon et al.[21] tested pre-LEV and newer gasoline vehicles and they concluded that SOA formation exceeds primary PM emissions. They also found lower SOA production from the newer vehicles compared to the pre-LEV gasoline vehicles and less SOA production during the hot-start testing compared to cold-start cycles. In another study, the authors confirmed the production of 15 times higher SOA compared to POA when they tested a gasoline vehicle over the New European Driving Cycle (NEDC).[22] Nordin et al.[23] showed that $C_6−C_9$ light aromatic hydrocarbons contributed up to 60% of the formed SOA when they tested Euro 1 and Euro 4 compliant passenger cars under idling conditions. Liu and co-workers[24] tested Euro 1 and Euro 4 gasoline vehicles under idling conditions and found that single-ring aromatics and naphthalene were responsible for 51−90% of the formed SOA.

Over the past decade the transportation sector has changed significantly with the introduction of gasoline direct injection (GDI) engines, driven by stringent legislative measures to lower vehicle fuel efficiency and greenhouse gas emissions. However, GDI engines are known to emit more soot emissions than traditional port fuel injection (PFI) engines.[25,26] In GDI engines, fuel is sprayed directly into the combustion chamber, which leads to incomplete fuel evaporation due to the imperfect mixing of fuel and air, resulting in pockets with high temperatures but insufficient oxygen, leading to pyrolysis reactions and soot formation. Additionally, as the fuel comes directly into contact with the cold cylinder walls and piston, a small amount of fuel may impinge on the piston, which during evaporation may lead to diffusion combustion and PM formation.[27−29] One strategy to reduce PM emissions from GDI vehicles is through the use of a gasoline particulate filter (GPF).[30,31] The use of GPFs in GDI vehicles have been shown to dramatically reduce PM mass, black carbon, and particle number emissions, as well as toxic pollutants such as polycyclic aromatic hydrocarbons (PAHs) and nitrated PAHs.[30,32] Despite the increased popularity of GDI engines in the light-duty vehicle sector across the U.S. and Europe, there is limited information on the SOA production from current technology GDI vehicles. In a recent study, Du et al.[33] tested both a PFI and GDI vehicle over the NEDC and reported much higher SOA production for the GDI vehicle compared to the PFI vehicle. In a different study, on the other hand, Zhao et al.[34] showed no differences in SOA production between PFI and GDI vehicles. Finally, Karjalainen et al.[35] tested a GDI vehicle over the NEDC and showed reduced SOA formation when the engine was warm and higher SOA formation during the cold-start phase when the three-was catalyst (TWC) was below its light-off temperature.

In this study, we investigated the SOA production from two current GDI vehicles with and without a catalyzed GPF. To the best of our knowledge, only Pieber et al.[36] evaluated SOA production from GDI vehicles equipped with prototype GPFs using a batch and a flow reactor. While the authors did not find differences in SOA formation with the tested noncatalyzed and catalytically coated GPFs, they suggested that the catalyzed GPFs could be installed at the same position as the underfloor TWC, and that this should be investigated in future work. Here, for the first time, we report results on SOA formation with catalyzed GPFs or 4-way catalysts when exercising GDI vehicles over the LA92 test cycle. This is a companion study to Yang et al.,[30] in which detailed primary gaseous and particulate emissions, as well as toxic pollutants, are reported.

■ EXPERIMENTAL SECTION

Test Vehicles and Driving Cycles. This study utilized two 2016 model year passenger cars. GDI_1 was equipped with a 2.0 L (L) wall-guided direct injection SI Atkinson cycle engine and GDI_2 was equipped with a 1.5 L downsized turbocharged centrally mounted direct injection engine. Testing on both vehicles was performed over duplicate cold-start LA92s cycles with commercial California E10 fuel. Additional information on the test vehicles and driving cycle can be found elsewhere.[30]

Both vehicles were tested in their original configuration and also retrofitted with a catalyzed GPF, which was installed in place of the underfloor TWC. The original close-coupled catalysts were retained in their stock location. The catalyzed GPFs were provided by the Manufacturers of Emissions Controls Association (MECA) and more information on their technical characteristics can be found in Yang et al.[30] Briefly, both GPFs were sized based on the engine displacement of each vehicle and they were catalyzed with precious metal loadings typical of underfloor catalysts matching the certification levels of the two vehicles. The GPFs had a TWC washcoat with approximately 1.0 g/Liter loading of palladium (Pd) and rhodium (Rh) (Pd:Rh tatio of 4:1).

Emissions and Chamber Testing. All tests were conducted in CE-CERT's Vehicle Emissions Research Laboratory (VERL), on a Burke E. Porter 48 in. single-roll electric dynamometer. A Pierburg Positive Displacement Pump-Constant Volume Sampling (PDP-CVS) system was used to obtain standard bag measurements for total hydrocarbons (THC), CO, NO_x, nonmethane hydrocarbons (NMHC), and carbon dioxide (CO_2). Bag measurements were made with a Pierburg AMA-4000 bench. More details for the measurement methods and analysis of the primary emissions are provided elsewhere.[30]

The photochemical aging experiments were carried out in UCR's (University of California, Riverside) Mobile Atmospheric Chamber (MACh). The MACh consists of a 30 m³ 2 mil fluorinated ethylene propylene Teflon film reactor. Briefly, the reactor is enclosed in a segmented, lightweight aluminum

frame fitted with wheels and a static resistant/UV blackout tarp. It is surrounded by 600 15 W, 18″, T8 black light fluorescent bulbs that serve as a photochemical light source. More detailed information on the construction and characterization of MACh can be found in Vu et al.[37]

Prior to each irradiation experiment, the chamber was cleaned by injecting O_3, H_2O_2, and purified air (AADCO 737 air purifier) and was irradiated with UV light. The AADCO air consists of no detectable reactive compounds (i.e., H_2O, NO_x, CO, O_3, hydrocarbons) to minimize background reactions in experiments. The chamber was then subsequently emptied and filled repeatedly until all gases and particles were measured to be below detection limit ($H_2O < -50$ °C dew point, NO_x, CO, HC, and O_3 at ∼0 ppb, and PM = 0 μg m^{-3}) then flushed with purified air overnight. Prior to the injection of vehicle exhaust, the chamber was half-filled with the AADCO air. CVS blank tests were conducted during the test campaign, with the chamber filled with the CVS air for the same duration as the LA92 cycle (1735 s) and then filled the remaining volume with the AADCO clean air. The final mass of aerosol formation (wall loss corrected) was found to average at 0.67 μg/m^3, which was then subtracted from the actual vehicle exhaust experiments.

The dilute exhaust was injected from the PDP-CVS into MACh during an LA92 cycle (excluding the hot soak). The exhaust was injected utilizing two Ejector Dilutors (Air-Vac TD11OH) in parallel, connected to a home-built clean air system with filters and desiccants to remove the PM (HEPA filters), water (silica gel columns), NO_x (Purafil), CO (Carulite canister), and hydrocarbons (activated charcoal) from the dilution air. The injection lines consisted of 8.5 m of 0.5″ stainless steel tubing. The dilution setup was designed to allow a variation of dilution from 50:1 up to 200:1 by varying the dilution air and CVS flow. MACh utilized gravitational forces to ensure a positive pressure inside the reactor, such that potential holes in the Teflon surface of the chamber will force air to flow out of the reactor. This minimized the contamination and dilution of the exhaust throughout the experiment.

For the experiments without the GPFs, after the exhaust was collected, the chamber was filled to maximum volume with purified air. A concentration of 1.0 ppm of H_2O_2 was also injected to act as an OH radical source. Prior to irradiation, the primary exhaust was evaluated for about 30 min to help characterize the diluted tailpipe composition. The emissions were then photo-oxidized continuously for 7−10 h. The exhaust was monitored during photo-oxidation utilizing a host of gaseous and particulate instruments allowing for real time evaluation of the aged exhaust. All chamber experiments were concluded when the wall-loss corrected aerosol mass formation, and the ozone concentration plateaued.

For the experiments with the GPF-equipped vehicles, the partially diluted exhaust collected in MACh was characterized for approximately 20−30 min. The total tailpipe PM were significantly lower and inert seeds were deemed necessary to mimic a similar condensable particulate surface area for low volatility gases to partition on as they age. Therefore, an ammonium sulfate (AS) seed was injected into the chamber utilizing an atomizer with a 2.40 M, aqueous AS solution (Acros, 99.5% in Millipore © DI water (18mΩ, < 100 ppb)), and subsequently heated and dried via silica gel. The dried seed was then passed through a 210Po neutralizer to minimize the fraction of charged particles. Experiments were seeded for

∼24.2 min. The aerosol was again classified to obtain a ratio of seed to tailpipe aerosol such that the total contribution of seed mass could be determined and ultimately subtracted from final secondary mass calculations. Finally, the remaining volume of the chamber was filled with AADCO purified air, and the remaining procedure was identical to the original configuration experiments. Ultimately, the condensable surface areas of the particles were within 15% and 5% on average between the stock and GPF tests for GDI_1 and GDI_2, respectively. The initial conditions for both vehicles with and without GPF are shown in Table S1 in the Supporting Information (SI).

MACh Instrumentation. Detailed information on the gas phase instrumentation is given in the SI. Dilution ratios were calculated by monitoring the CO_2 concentrations of the exhaust, dilution air, and initial experimental concentration. The equations utilized to calculate the dilution ratios are provided in the SI. Particle phase instrumentation included a commercial scanning mobility particle sizer (SMPS) consisting of a TSI 3080 Electrostatic Classifier, TSI 3081 long column Differential Mobility Analyzer (DMA) column, and a TSI ultrafine condensation particle counter (CPC) 3776. The 3776 CPC was operated in "low flow mode" with a sample flow of 0.3 LPM and the sheath flow was set to 3.0 LPM. The SMPS measured electrical mobility diameters from 14.6 to 661.2 nm.

Black carbon mass was measured with an AVL Micro Soot Sensor (MSS) with a high power laser diode operating at 802 nm with a photoacoustic sensor. For the chemical composition of aerosol, an Aerodyne high-resolution time-of-flight aerosol mass spectrometer (HR-ToF-AMS) was used.[38] The HR-ToF-AMS provided real-time information on the nonrefractory aerosol, including sulfate, nitrate, ammonium, chloride, and organic.[39] The HR-ToF-AMS was operated in both V and W modes, and the data processing was completed using the ToF-AMS Analysis Toolkit 1.57 and ToF-AMS HR analysis 1.16. The Unit Mass Resolution (UMR) and HR Frag table for CO_2 were altered from the assumed concentration of 370 ppm to the measured CO_2 concentration using a LI-COR LI-840A CO_2/H_2O analyzer. Using the HR-ToF-AMS, the organic, ammonium, nitrate, and sulfate ratios were calculated and applied to the total mass calculated utilizing volume calculated from the SMPS and the density from the aerosol particle mass (APM) analyzer (after subtracting the black carbon contribution). Thus, the estimated mass is reflective of the mass of particles less than 500 nm in diameter; if particles exist at largest sizes than the reported mass, likely under-predicts the total mass of particles. Wall loss corrected black carbon mass was assumed to be constant throughout irradiation experiment.

A home-built, tandem differential mobility analyzer (TDMA) consisting of two TSI 3081 DMAs and a TSI model 3760A CPC provided volatility measurements.[40] The first column selects a particle electrical mobility diameter, typically at the peak mode. The size selected particles then travel through a heated column (100 °C) with a residence time of ∼17 s. The heated aerosol is then classified by scanning mode via the second DMA column such that a new size distribution of the aerosol is measured. The initial diameter is then compared to the final diameter to obtain the volume fraction remaining (VFR) of the particles (i.e.,

$$VFR = \frac{volume_{final}}{volume_{initial}},$$ assuming a spherical aerosol). Classified particle size changes with the peak diameter during the experiments. As the peak shifts throughout the irradiation experiment, so does the selected diameter in the first DMA.
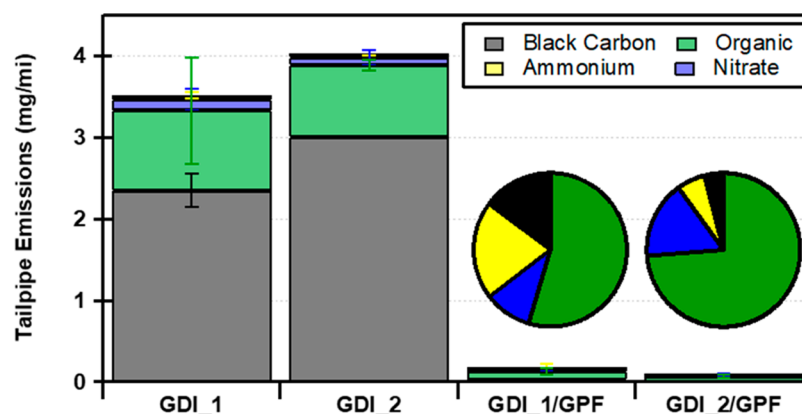
Figure 1. Composition of tailpipe PM for GDI_1 and GDI_2. Pie charts display PM composition for GPF configurations. Organic material was considered POA.
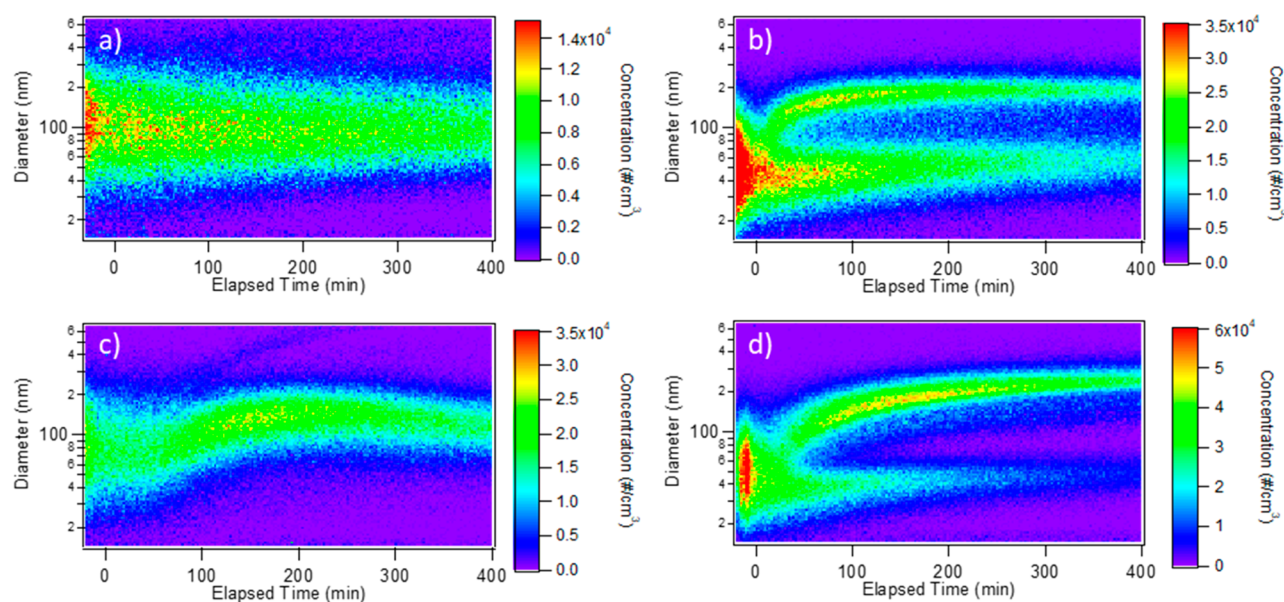
Figure 2. (a−d). Electrical mobility size distribution image plots for GDI_1 (a), GDI_1/GPF (b), GDI_2 (c), and GDI_2/GPF (d) measured with the SMPS. $t = 0$ corresponds to illumination of UV lights.

A Kanomax APM analyzer system was used to measure particle effective density. The APM was paired with a home-built SMPS. Particles were initially selected by mass and later passed through a scanning DMA column where an effective density based on the electrical mobility diameter was calculated. The APM has the ability to select aerosol with a mass from 0.30 to 50.0 fg, which is equivalent to a particle of unit density with a diameter of 50−400 nm. A more detailed summary of the APM-SMPS system is described in an earlier study.[41]

SMPS data was used for the calculation of the volume of aerosol during the irradiation experiments. All SMPS data was corrected for particle wall losses using first order wall loss kinetics, as described in detail by Cocker et al.[42] Vapor wall losses have been assumed and measured to be insignificant in past chamber experiments.[37] From the volume, mass was calculated by using effective density measurements. Final mass calculations were determined from the effective density and volume calculated at the end of the irradiation experiments.

■ RESULTS AND DISCUSSION

Tailpipe PM Mass Composition. Figure 1 shows the PM mass and composition emitted directly from the tailpipe. PM emissions for GDI_1 were lower compared to GDI_2. Both vehicles emitted tailpipe PM of similar composition, with 67% and 74% of the PM emissions consisting of black carbon, 28% and 22% of POA, and the remaining 5% of ammonium and nitrate for GDI_1 and GDI_2, respectively. These results are in agreement with previous studies showing that GDI PM are primarily black carbon in nature.[43,44]

The use of the catalyzed GPFs with both vehicles resulted in 95% and 98% reductions in total tailpipe PM mass emissions for GDI_1/GPF and GDI_2/GPF, respectively. For both vehicles, the GPFs efficiently removed black carbon emissions, with removal efficiencies reaching over 99.8%, and considerably altered the average aerosol fraction composition. Black carbon comprised of 15% and 4% of the total tailpipe PM for GDI_1/GPF and GDI_2/GPF, respectively. POA was also significantly reduced with the use of GPFs, but not at the same removal efficiency compared to black carbon. This phenomenon is likely due to varying volatilities of the VOCs emitted.[36]
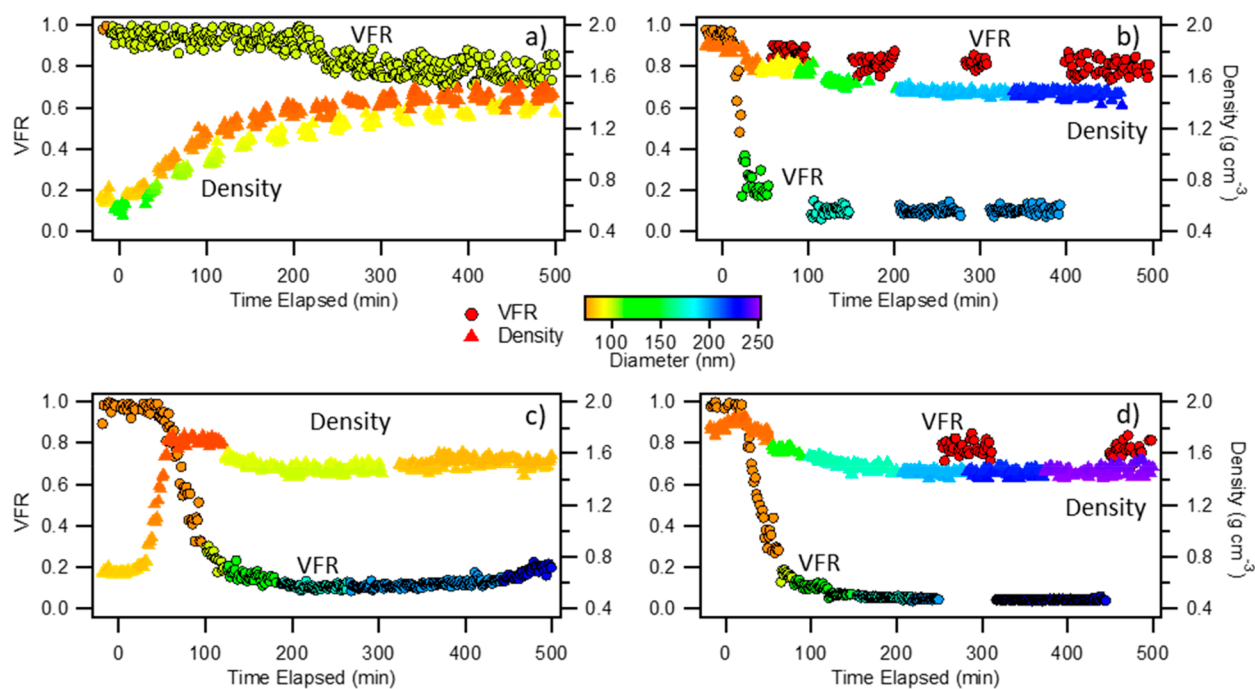
Figure 3. (a−d). Volume fraction remaining (left *y*-axis) and the effective density (right *y*-axis) for GDI_1 (a), GDI_1/GPF (b), GDI_2 (c), and GDI_2/GPF (d). Color scale relates to electrical mobility diameter selected

The hot, lower volatility gases, remain in the gas phase through the catalyzed GPF, but as the emissions dilute and cool, the same lower volatility organic gases condense onto existing particles. This organic material, although emitted as a gas, condensed without any reaction and is therefore measured as POA. While POA mass reduced with the GPF, the average percentage contribution of the POA mass to total PM mass increased. POA mass comprised of 55% for GDI_1/GPF and 74% for GDI_2/GPF of the total PM, with the remaining 20−30% of the primary aerosol consisting of ammonium and nitrate.

Particle Size Distributions. Figure 2(a−d) shows the electrical mobility size distribution and evolution of the aerosol during the irradiation experiments. GDI_1 showed a decisively unimodal distribution, peaking at 95 nm with an effective density of approximately 0.58 g cm^{-3}, as shown in Figure 3a. The effective density is consistent with fractal black carbon particles.[45] As the emissions aged, no notable shift in electrical mobility diameter was observed, but the aerosol mass increased by ~2.5 times. This increase in the aerosol mass was attributed to the increase of the effective density of particles in the ~100 nm range. For GDI_1, particle number concentrations above 200 nm were small and therefore effective density measurements were not available in this range.

During the aging testing for GDI_2, a shift in the particle electrical mobility diameter of the main distribution was seen, as shown in Figure 2c. Similar to GDI_1, the tailpipe aerosol consisted of a broad, unimodal peak centering at ~75 nm with a density of 0.67 g cm^{-3}, which is consistent with fractal black carbon (Figure 3c). As gases condensed during the irradiation experiment, the broad peak sharpened and shifted to ~120 nm. The density of the aerosol quickly increased to ~1.70 g cm^{-3} (*t* = 75 min). This change in density was indicative of ammonium nitrate condensation (1.72 g cm^{-3}) onto the black carbon particle backbone. After ~100 min, the contribution of less dense SOA to total aerosol mass increased, thus decreasing the

effective density to 1.53 g cm^{-3} (*t* = 200 min). A small number of particles grew outside of the main distribution at *t* ~ 75 min, and eventually grew out of the detection limit of the SMPS at *t* ~ 250 min. Because of this, the volumes calculated from the SMPS data for GDI_2 experiments were corrected from ~250 min and onward, by calculating the contribution of each mode to total volume. This ratio was then applied through the duration of the experiment which likely resulted in a slight underproduction in the total mass formed. The underestimation is expected to be minimal as the particle mass formation of the smaller peak plateaued at 280 min, indicating aerosol mass formation had completed.

For the GPF equipped vehicles, the initial effective density of the tailpipe aerosol was roughly the same at ~0.96 g cm^{-3}, indicating the presence of a fractal black carbon particle backbone, but increased fractional POA composition when compared to the stock configuration exhaust (Figure 3b and d). For both vehicles, the initial distribution in the irradiation experiments includes an ammonium sulfate seed, which peaked at 50 nm with densities being consistent with that of ammonium sulfate at ~1.78 g cm^{-3} (Figure 2b and d). The seed to primary aerosol ratio (volume) was 24.6 and 11.4 for GDI_1/GPF and GDI_2/GPF, respectively. The aging of the aerosol resulted in the formation of a bimodal particle distribution, with peak modes at ~230 and 50 nm for both vehicles. At the end of the irradiation experiments the aerosol density for both vehicles was ~1.49 g cm^{-3}, consistent with the composition of the ammonium sulfate seed (1.77 g cm^{-3}), ammonium nitrate (1.72 g cm^{-3}), and SOA (~1.40 g cm^{-3}). The distinguishing criteria between the experiments of the two GPF vehicles was the number of particles in the larger diameter peak, which drastically changed the total mass calculated when comparing the emissions from both vehicles.

Figure 3(a−d) also presents the volume fraction remaining (VFR) of the aerosol during the irradiation experiment. In all four experimental conditions, the initial VFR was equal to 1.0.
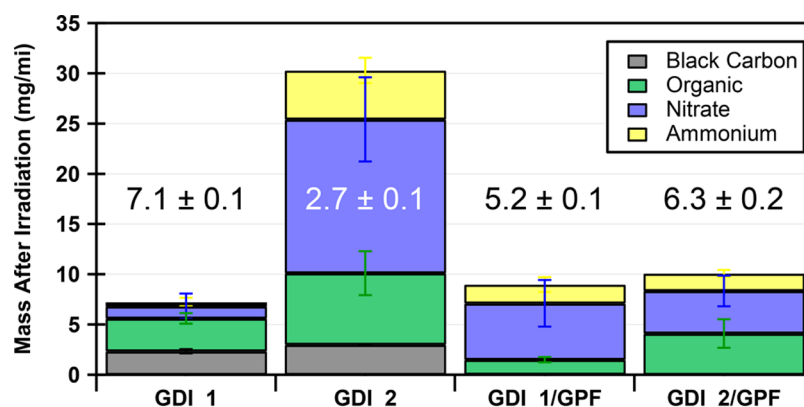
Figure 4. Aerosol mass and chemical composition at the conclusion of the irradiation experiment. Values across graph represent the average VOC:NO$_x$ (ppm$_v$:ppm$_v$) ratio.

This value was consistent with nonvolatile black carbon (original configuration experiments) and ammonium sulfate seed (GPF experiments). The VFR for GDI_1 was unique when compared to GDI_2 with and without GPF due to the high VFR throughout the experiment. This phenomenon can be explained by the nature of the fractal black carbon seed particles and the relatively small amount of secondary aerosol formed. When the gas-to-particle phase partitioning occurred, the void space of the fractal black carbon backbone filled, which increased the mass of the aerosol, but had no effect on the electrical mobility diameter. Therefore, even if the additional aerosol mass formed was volatile when heated, the fractal black carbon backbone remained which resulted in a VFR value of around 1.0. Once the density reached ~1.40 g cm-3, the VFR dropped from 1.0 to ~0.8. This indicated the particle's morphology was more sphere-like, and the additional condensation of SOA resulted in a decreasing VFR, which was also confirmed with the HR-ToF-AMS results discussed in the following section (Figure 4). Similar findings have been reported by Nakao et al.,[45] when they investigated the aging of diesel exhaust. For GDI_2, the aerosol mass that condensed onto the initial black carbon was found to be completely volatile at 100 °C, resulting in a VFR of ~0.10. The initial aerosol that condensed was predominantly inorganic ammonium nitrate, but also comprised of SOA (as shown in Figure 4). As the organic gases continued to age and condense, the contribution of SOA to the total mass in the experiment increased, ultimately increasing the VFR to ~0.25.

Both GPF equipped vehicles followed similar trends to GDI_2. The low diameter mode maintained similar properties to the ammonium sulfate seed with a high VFR. There was evidence of condensation of gases onto the smaller mode of particles as the VFR dropped to around 0.8, which was an indication of ammonium nitrate and SOA mass condensation. The large diameter mode displayed properties indicative to an ammonium nitrate and SOA dominated aerosol (VFR ~ 0.10). The larger mode for both GPF vehicles was closely related to the GDI_2 aerosol profile (Figure 2c), with a similar composition (Figure 4).

Aerosol Composition. Figure 4 shows the measured aerosol mass composition after 400 min of irradiation in the atmospheric chamber (primary and secondary aerosol combined). The values shown on the graph indicate the VOC to NO$_x$ ratios (SI Table S1) in the experiments. GDI_1 formed the least amount of total aerosol compared to the other vehicles. The total aerosol after irradiation was 7.24 mg/mile,

with approximately 45% of the aerosol composition comprised of organics. GDI_2 formed the highest amount of total aerosol at 30.3 mg/mile, with GDI_1 forming the lowest at 7.2 mg/mile. The majority of the aerosol formed after irradiation was inorganic in nature (ammonium nitrate), with only 23.5% of the total aerosol being organic. Ammonium nitrate is formed when nitric acid (formed through the oxidation of NO$_x$) homogeneously reacts with gaseous NH$_3$.[46] The total formation of salt will depend on the concentration of NO$_x$, and NH$_3$ (not measured for these experiments) emitted from the tailpipe. For GDI_2 the VOC to NO$_x$ ratio was the lowest compared to other vehicles due to the high NO$_x$ emissions from this vehicle.[30] A VOC to NO$_x$ ratio of 2.7 is relatively low and considered to be in a VOC limited regime for secondary chemistry in relation to ozone production.[47]

The total aerosol formed for the GPF vehicles after the irradiation experiments showed different trends. For GDI_1/GPF, the mass of ammonium nitrate increased when compared to the experiments without GPF. This increase in the ammonium nitrate mass was likely due to the higher NO$_x$ and NH$_3$ concentrations with the GPF. Although the catalyzed GPF reduced tailpipe NO$_x$ emissions by 16.6%,[30] the difference in dilution ratios between the two sets of experiments (60 for the GPF testing vs 105 for the non-GPF testing) resulted in the formation of more ammonium nitrate in the chamber for the GPF tests. It was theorized that if the dilution ratio was constant between experimental conditions, the ammonium nitrate formation would have followed similar patterns with tailpipe NO$_x$ emissions. For GDI_2/GPF, the ammonium nitrate was lower than the concentration of the original configuration. Concentrations of NO$_x$ both in the tailpipe and in the chamber for this vehicle without the catalyzed GPF were considerably higher than those with the GPF configuration, despite the dilution ratios utilized. As shown in our previous study, the total reduction in NO$_x$ emissions for GDI_2/GPF was 87.6%.[30] Overall, the role of NH$_3$ should be further investigated in GDI vehicles with and without GPFs, as it may significantly contribute to the production of secondary inorganic aerosols mainly in the form of ammonium nitrate. Ammonia could be produced in the front TWC from engine-out NO$_x$ and generated H$_2$ through water−gas-shift and HC steam reforming reactions.[48,49] The NH$_3$ from the front TWC will either pass through the underfloor TWC/GPF system or be oxidized to N$_2$O, NO$_x$ or N$_2$. While NH$_3$ emissions measurements were not made possible for this study, it is reasonable to assume that
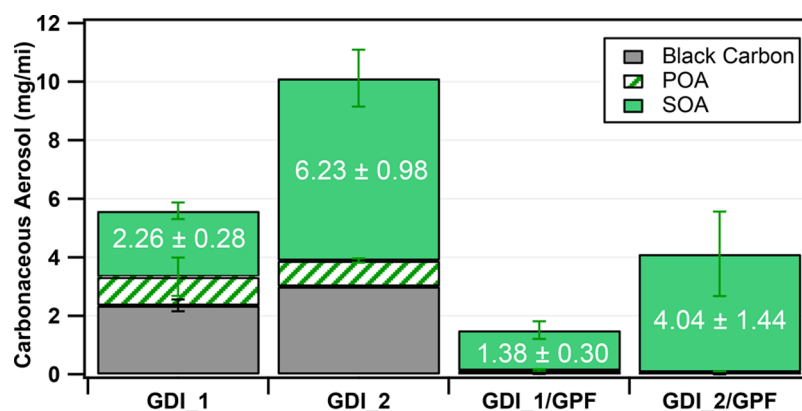
Figure 5. Total carbonaceous aerosol composition (black carbon, POA, and SOA) at the conclusion of the irradiation experiments. Values indicate SOA formation, expressed in mg/mile.
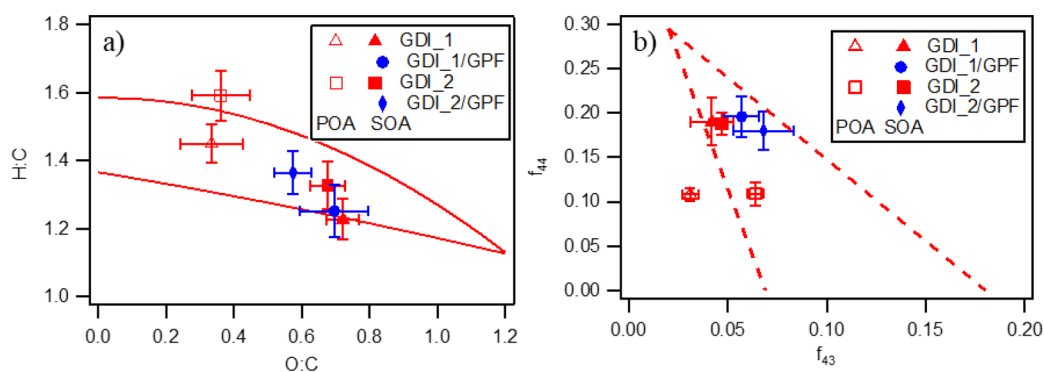
Figure 6. High resolution AMS results for H:C, O:C ratios for POA (without GPFs) and SOA (with and without GPFs) for GDI_1 and GDI_2 (left panel); f_{44} and f_{43} relationships for the POA (without GPFs) and SOA (with and without GPFs) for GDI_1 and GDI_2 (right panel).

the differences in the oxygen storage component (OSC) materials levels of the GPF versus the TWC was the most likely cause of the difference in the amount of NH_3 at the tailpipe.

Figure 5 shows the contribution of black carbon, POA, and SOA to the total carbonaceous aerosol at the end of the irradiation experiments. The addition of the GPF resulted in 73% and 59% lower total carbonaceous aerosol (black carbon, POA, and SOA) for GDI_1 and GDI_2, respectively. For all experiments, there was a larger estimated mass of SOA formed compared to the POA mass, ranged from 2.3 to 60 times. Both vehicles without the catalyzed GPF produced more SOA than with the GPF configuration, with GDI_2 showing significantly higher SOA production than GDI_1. The reductions in SOA formed with the addition of a GPF were 39% and 35%, respectively, for GDI_1/GPF and GDI_2/GPF. In a previous study by Pieber et al.[36] it was reported that the use of GPF did not result in reductions in the gas phase pollutants responsible for SOA formation. It should be noted, however, that in that study the GPF was not designed to replace the original TWC. The results reported here showed that in addition to the removal of tailpipe PM, the catalyzed GPFs were more efficient in the removal of gas phase pollutants, such as NMHC, which are contributing factors to SOA production.[30] The main reason for this observation may be the fact that the wall flow design of the GPF, having alternate channels plugged, forces the exhaust to pass through the catalyst coated on the wall of the filter and increasing the contact with the catalyst. In a standard underfloor catalyst made up of a completely open honeycomb

design, the contact and reaction is concentrated at the wall surface and may slip in some operating regimes.

Another distinction between the properties of the POA and SOA is the oxygen content in the organic aerosol, which can be derived from the high resolution data of the AMS. Two important measures of this are fraction of the mass to charge ratio, total normalized ion fragments of m/z 44 (CO_2^+) versus m/z 43 ($C_2H_3O^+$), and the molar oxygen to carbon ratio (molar), as shown in Figure 6.[38] Although the GPF vehicles did not emit sufficient amount of tailpipe aerosol to quantify the POA properties, the SOA values are still shown in Figure 6. Average oxygenated organic aerosol (OOA) typically has an O:C ratio of 0.5 to 0.9; with semivolatile OOA (SV-OOA) classified with an O:C of 0.4−0.6, and low-volatility OOA (LV-OOA) from 0.7 to 1.0.[12] The POA for GDI_1 and GDI_2 showed an average O:C ratio of ∼0.35. As the aerosol aged and the organic aerosol fraction increased, the O:C ratio increased to an average of 0.67, indicating the final organics were more oxidized than the tailpipe OA. Our results compare well to previous studies conducted on gasoline vehicles and reported O:C ratios from 0.3 to 0.7.[23,24,50] The slopes from the POA to the SOA were found to be −0.58 and −0.83 for GDI_1 and GDI_2, respectively. A slope of −1.0 designates the addition of an alcohol or peroxide, and a slope of −0.5 and 0 indicate the addition of a carboxylic acid with and without fragmentation, respectively.[51] The slopes in this study are comparable to those found in other studies for gasoline vehicle exhaust[23,50] and showed that SOA production could be explained by a combination of the addition of both alcohol/peroxide and carboxylic acid (with and without C−C bond cleavage).[51,52]
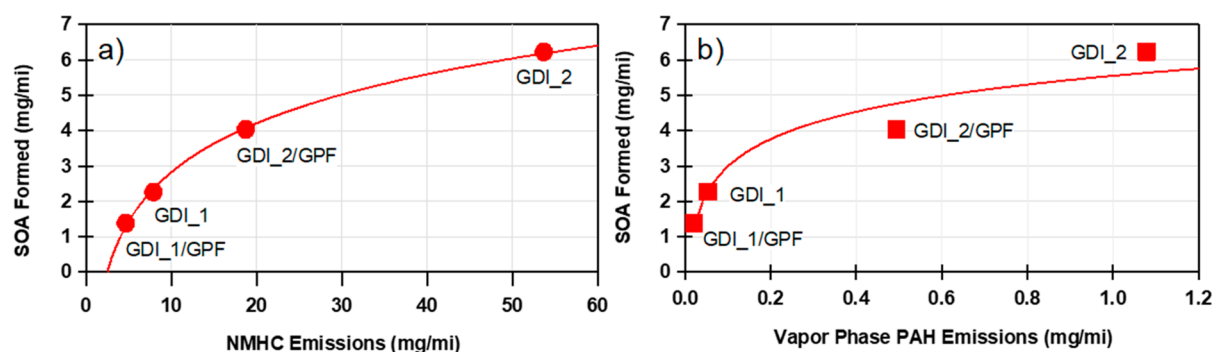
Figure 7. (a,b). SOA mass relationships to (a) NMHC emissions, and (b) Vapor phase PAH emissions for both GDI vehicles with and without and GPFs.

Another method used to measure the amount of oxidation in the aerosol is the f_{44} (ratio of m/z 44 to total signal in the component mass spectrum) and f_{43} (defined similarly to f_{44}). SV-OOA typically has an f_{44} from 0.03 to 0.12, while the LV-OOA is typically in the 0.13−0.21 range.[23] It has also been found that the majority of the atmospheric aerosols fall within the triangle developed by Ng et al.,[51] depicted in Figure 6. For both vehicles without the GPF, POA started with an f_{44} of ~0.11 and increased to an average of 0.19, suggesting the SOA formed was highly oxidized and likely to contain polyacidic or acid-derived moieties. For the GPF vehicles, SOA had similar compositional fraction of f_{44} and f_{43} compared to the original configurations. The fraction of total organic signal found in this work fell in the LV-OOA region (upper portion of the triangle shown in Figure 6) and exceeded other f_{44} found in previous studies conducting experiments with gasoline vehicles, which varied from 0.10[24,50] up to 0.15,[23] indicating the aerosol formed was highly oxidized.

The difference in SOA production between the test vehicles, reveals that the engine design and possibly calibration played some role in both the primary and secondary emissions formation. In addition to primary PM mass emissions,[30] GDI_2 also produced more SOA compared to GDI_1. GDI_1 was characterized by a relatively high compression ratio (14.0:1) relative to GDI_2 (10.0:1) that is typically higher than those found in commercially available passenger car GDI engines. The higher compression ratio for GDI_1 led to a homogeneous mixture for fuel with air due to more time for perfect mixture preparation, as well as to higher in-cylinder temperatures, hence higher flame temperatures during combustion to suppress PM and assist to a more complete oxidation of particles, particularly the volatile organic fraction. Additionally, the close contact between fuel and oxygen and the increasing wall temperatures due to increasing combustion temperatures will likely increase the heat flux and hence will result in less unburned hydrocarbons, which can be precursors for SOA production.

Primary emissions of NMHC from light-duty GDI vehicles have been extensively measured.[25,30,44] Here we show the impact of NMHC emissions in the enhancement of SOA production (Figure 7a). A decrease in measured NMHC tailpipe concentration results in a decrease in potential SOA formation. In addition to the engine design, the order of magnitude difference in NMHC emissions can also be explained by the differences in the certification levels. GDI_1 was certified to LEVIII SULEV30 and GDI_2 to LEVII. Therefore, the lower SOA production with GDI_1 was a

consequence of the substantially lower POA emissions for this vehicle compared to GDI_2. Previous studies have also shown lower SOA with newer, lower emitting vehicles than older, higher emitting vehicles.[21] Formation of SOA also correlates with the vapor-phase total PAH emissions. Using our previously published data by Yang et al.,[30] it can be observed that the total vapor-phase PAH emissions drives potential SOA formation, as shown in Figure 7b. As shown in Yang et al.,[30] vapor-phase PAH emissions were dominated by two-ring and three-ring aromatic species, mainly naphthalenes and methyl/ethyl-naphthalenes, and phenanthrene. These low molecular weight PAH compounds are known for their crucial role for the production of SOA.[10,53,54] These results are consistent with our current knowledge of SOA formation from vehicular exhaust. Additional work is required to develop mechanistic models that lead to aerosol formation from NMHC and PAH emissions.

Implications. Vehicular emissions are an important source of SOA precursors in urban areas. The widespread penetration of GDI engines in the US and European markets, that are known to emit more PM and black carbon emissions than PFI engines, will likely alter SOA formation and affect urban air quality and climate. It is expected that the addition of catalyzed GPFs on GDI vehicles in regions of the world that have technology forcing particle number regulations, will significantly reduce tailpipe PM and black carbon emissions, and will help reduce VOC emissions that act as SOA precursors. The results reported here showed that the catalyzed GPF was most efficient in the removal of the accumulation mode particles and black carbon aerosol. The GPF was quite efficient in the removal of POA as well, however, due to volatility effects with the cooling of the exhaust, a greater POA fraction was observed relative to the original configuration.

We showed that when particles were fractal (black carbon), the condensation of low volatility gases would not change the secondary aerosol particle mobility diameter until the aerosol became spherical, with a density of 1.4 g cm^3. Our results are important because the measurement of effective density for more accurate prediction of secondary aerosol mass is vital due to significant changes in effective density in the same irradiation experiment and intravehicle variability. For the same irradiation experiment, multiple particle modes of different compositions may exist, leading to varying characteristics such as density and volatility.

Our results confirmed previous studies showing considerable secondary aerosol formation after irradiation. The use of catalyzed GPFs will likely reduce NMHC emissions, which are

SOA precursors, as well as the total carbonaceous aerosol from vehicle exhaust. When comparing vehicle technologies (LEVII for GDI_2 and LEVIII for GDI_1), there was a 13% reduction in tailpipe mass. However, the considerable decrease in reactive gas emissions resulted in a 76% reduction for the estimated total secondary aerosol formation. This difference may be amplified by the difference in dilution ratios of the experiments under the present test conditions compared to actual dilution in the atmosphere. Regulatory actions should be taken toward the reduction of gas-phase emissions, which may lead to the reduction of submicron atmospheric aerosol mass. We can confidently conclude that the application of catalyzed GPFs in GDI engines will have substantial benefits in both the tailpipe emissions and SOA production, even for vehicles certified to higher emission limits (i.e., LEVII).

■ ASSOCIATED CONTENT

ⓢ Supporting Information

The Supporting Information is available free of charge on the ACS Publications website at DOI: 10.1021/acs.est.8b06418.

> Further details on the experimental procedures and data analyses (PDF)

■ AUTHOR INFORMATION

Corresponding Authors

*(G.K.) Phone: (951)-781-5799; fax: (951)-781-5790; e-mail: gkaraval@cert.ucr.edu.

*(A.A.-A.) Phone: (301)-405-8527; e-mail: asaawku@umd.edu.

ORCID Ⓞ

Jiacheng Yang: 0000-0002-9442-9267

Emmanuel Fofie: 0000-0003-1241-2910

Georgios Karavalakis: 0000-0001-5011-8371

Notes

The authors declare no competing financial interest.

■ REFERENCES

(1) Heal, M. R.; Kumar, P.; Harrison, R. M. Particles, air quality, policy and health. *Chem. Soc. Rev.* **2012**, *41*, 6606−6630.

(2) Dallmann, T. R.; Onasch, T. B.; Kirchstetter, T. W.; Worton, D. R.; Fortner, E. C.; Herndon, S. C.; Wood, E. C.; Franklin, J. P.; Worsnop, D. R.; Goldstein, A. H.; Harley, R. A. Characterization of particulate matter emissions from on-road gasoline and diesel vehicles using a soot particle aerosol mass spectrometer. *Atmos. Chem. Phys.* **2014**, *14*, 7585−7599.

(3) McDonald, B. C.; Dallmann, T. R.; Martin, E. W.; Harley, R. A. Long-term trends in nitrogen oxide emissions from motor vehicles at national, state, and air basin scales. *J. Geophys Res-Atmos* **2012**, *117*, D00V18.

(4) McDonald, B. C.; Gentner, D. R.; Goldstein, A. H.; Harley, R. A. Long-term trends in motor vehicle emissions in U.S. urban areas. *Environ. Sci. Technol.* **2013**, *47*, 10022−31.

(5) California Air Resources Board, https://www.arb.ca.gov/desig/adm/adm.htm.

(6) May, A. A.; Presto, A. A.; Hennigan, C. J.; Nguyen, N. T.; Gordon, T. D.; Robinson, A. L. Gas-particle partitioning of primary organic aerosol emissions: (1) Gasoline vehicle exhaust. *Atmos. Environ.* **2013**, *77*, 128−139.

(7) Samet, J. M.; Dominici, F.; Curriero, F. C.; Coursac, I.; Zeger, S. L. Fine particulate air pollution and mortality in 20 US cities, 1987 − 1994. *N. Engl. J. Med.* **2000**, *343*, 1742−1749.

(8) Lelieveld, J.; Evans, J. S.; Fnais, M.; Giannadaki, D.; Pozzer, A. The contribution of outdoor air pollution sources to premature mortality on a global scale. *Nature* **2015**, *525*, 367−371.

(9) Pope, C. A.; Burnett, R. T.; Thun, M. J.; Calle, E. E.; Krewski, D.; Ito, K.; Thurston, G. D. Lung cancer, cardiopulmonary mortality, and long-term exposure to fine particulate air pollution. *JAMA* **2002**, *287*, 1132−1141.

(10) Odum, J. R.; Junkkamp, T. P.; Griffin, W. R.; Forstner, H. J. L.; Flagan, R. C.; Seinfeld, J. H. Aromatics, reformulated gasoline, and atmospheric organic aerosol formation. *Environ. Sci. Technol.* **1997**, *31*, 1890−1897.

(11) Gentner, D. R.; Jathar, S. H.; Gordon, T. D.; Bahreini, R.; Day, D. A.; Haddad, I. E.; Haynes, P. L.; Pieber, S. M.; Platt, S. M.; De Gouw, J.; Goldstein, A. H.; Harley, R. A.; Jimenez, J. L.; Prevot, A. S. H.; Robinson, A. L. Review of urban secondary organic aerosol formation from gasoline and diesel motor vehicle emissions. *Environ. Sci. Technol.* **2017**, *51*, 1074−1093.

(12) Jimenez, J. L.; Canagaratna, M. R.; Donahue, N. M.; Prevôt, A. S. H.; Zhang, Q.; Kroll, J. H.; Decarlo, P. F.; Allan, J. D.; Coe, H.; Ng, N. L.; Aiken, A. C.; Ulbrich, I. M.; Grieshop, A. P.; Duplissy, J.; Wilson, K. R.; Lanz, V. A.; Hueglin, C.; Sun, Y. L.; Tian, J.; Laaksonen, A.; Raatikainen, T.; Rautiainen, J.; Vaattovaara, P.; Ehn, M.; Kulmala, M.; Tomlinson, J. M.; Cubison, M. J.; Dunlea, E. J.; Alfarra, M. R.; Williams, P. I.; Bower, K.; Kondo, Y.; Schneider, J.; Drewnick, F.; Borrmann, S.; Weimer, S.; Demerjian, K.; Salcedo, D.; Cottrell, L.; Takami, A.; Miyoshi, T.; Shimono, A.; Sun, J. Y.; Zhang, Y. M.; Dzepina, K.; Sueper, D.; Jayne, J. T.; Herndon, S. C.; Williams, L. R.; Wood, E. C.; Middlebrook, A. M.; Kolb, C. E.; Baltensperger, U.; Worsnop, D. R. Evolution of organic aerosols in the atmosphere. *Science* **2009**, *326*, 1525−1529.

(13) Hallquist, M.; Wenger, J. C.; Baltensperger, U.; Rudich, Y.; Simpson, D.; Claeys, M.; Dommen, J.; Donahue, N. M.; George, C.; Goldstein, A. H.; Hamilton, J. F.; Herrmann, H.; Hoffmann, T.; Iinuma, Y.; Jang, M.; Jenkin, M. E.; Jimenez, J. L.; Kiendler-Scharr, A.; Maenhaut, W.; McFiggans, G.; Mentel, Th. F.; Monod, A.; Prévôt, A. S. H.; Seinfeld, J. H.; Surratt, J. D.; Szmigielski, R.; Wildt, J. The formation, properties and impact of secondary organic aerosol: current and emerging issues. *Atmos. Chem. Phys.* **2009**, *9*, 5155−5236.

(14) Hu, W.; Hu, M.; Hu, W.; Jimenez, J. L.; Yuan, B.; Chen, W.; Wang, M.; Wu, Y.; Chen, C.; Wang, Z.; Peng, J.; Zeng, L.; Shao, M. Chemical composition, sources, and aging process of submicron aerosols in Beijing: Contrast between summer and winter. *J. Geophys. Res.-Atmos.* **2016**, *121*, 1955−1977.

(15) Zhang, Q.; Jimenez, J. L.; Canagaratna, M. R.; Allan, J. D.; Coe, H.; Ulbrich, I.; Alfarra, M. R.; Takami, A.; Middlebrook, A. M.; Sun, Y. L.; Dzepina, K.; Dunlea, E.; Docherty, K.; DeCarlo, P. F.; Salcedo, D.; Onasch, T.; Jayne, J. T.; Miyoshi, T.; Shimono, A.; Hatakeyama, S.; Takegawa, N.; Kondo, Y.; Schneider, J.; Drewnick, F.; Borrmann, S.; Weimer, S.; Demerjian, K.; Williams, P.; Bower, K.; Bahreini, R.; Cottrell, L.; Griffin, R. J.; Rautiainen, J.; Sun, J. Y.; Zhang, Y. M.; Worsnop, D. R. Ubiquity and dominance of oxygenated species in

organic aerosols in anthropogenically-influenced Northern Hemisphere mid latitudes. *Geophys. Res. Lett.* **2007**, *34*, L13801.

(16) Bahreini, R.; Middlebrook, A. M.; de Gouw, J. A.; Warneke, C.; Trainer, M.; Brock, C. A.; Stark, H.; Brown, S. S.; Dube, W. P.; Gilman, J. B.; Hall, K.; Holloway, J. S.; Kuster, W. C.; Perring, A. E.; Prevot, A. S. H.; Schwarz, J. P.; Spackman, J. R.; Szidat, S.; Wagner, N. L.; Weber, R. J.; Zotter, P.; Parrish, D. D. Gasoline emissions dominate over diesel in formation of secondary organic aerosol mass. *Geophys. Res. Lett.* **2012**, *39*, L06805.

(17) McDonald, B. C.; Goldstein, A. H.; Harley, R. A. Long-term trends in California mobile source emissions and ambient concentrations of black carbon and organic aerosol. *Environ. Sci. Technol.* **2015**, *49*, 5178−5188.

(18) Saliba, G.; Saleh, R.; Zhao, Y.; Presto, A. A.; Lamber, A. T.; Frodin, B.; Sardar, S.; Maldonado, H.; Maddox, C.; May, A. A.; Drozd, G. T.; Goldstein, A. H.; Russell, L. M.; Hagen, F.; Robinson, A. L. Comparison of gasoline direct-injection (GDI) and port fuel injection (PFI) vehicle emissions: Emission Certification standards, cold-start, secondary organic aerosol formation potential, and potential climate impacts. *Environ. Sci. Technol.* **2017**, *51*, 6542−6552.

(19) Ma, P.; Zhang, P.; Shu, J.; Yang, B.; Zhang, H. Characterization of secondary organic aerosol from photo-oxidation of gasoline exhaust and specific sources of major components. *Environ. Pollut.* **2018**, *232*, 65−72.

(20) Zhao, Y.; Saleh, R.; Saliba, G.; Presto, A. A.; Gordon, T. D.; Drozd, G. T.; Goldstein, A. H.; Donahue, N. M.; Robinson, A. L. Reducing secondary aerosol formation from gasoline vehicle exhaust. *Proc. Natl. Acad. Sci. U. S. A.* **2017**, *114*, 6984−6989.

(21) Gordon, T. D.; Presto, A. A.; May, A. A.; Nguyen, N. T.; Lipsky, E. M.; Donahue, N. M.; Gutierrez, A.; Zhang, M.; Maddox, C.; Rieger, P.; Chattopadhyay, S.; Maldonado, H.; Maricq, M. M.; Robinson, A. L. Secondary organic aerosol formation exceeds primary particulate matter emissions for light-duty gasoline vehicles. *Atmos. Chem. Phys.* **2014**, *14*, 4661−4678.

(22) Platt, S. M.; El Haddad, I.; Zardini, A. A.; Clairotte, M.; Astorga, C.; Wolf, R.; Slowik, J. G.; Temime-Roussel, B.; Marchand, N.; Ježek, I.; Drinovec, L.; Močnik, G.; Möhler, O.; Richter, R.; Barmet, P.; Bianchi, F.; Baltensperger, U.; Prévôt, A. S. H. Secondary organic aerosol formation from gasoline vehicle emissions in a new mobile environmental reaction chamber. *Atmos. Chem. Phys.* **2013**, *13*, 9141−9158.

(23) Nordin, E. Z.; Eriksson, A. C.; Roldin, P.; Nilsson, P. T.; Carlsson, J. E.; Kajos, M. K.; Hellén, H.; Wittbom, C.; Rissler, J.; Löndahl, J.; Swietlicki, E.; Svenningsson, B.; Bohgard, M.; Kulmala, M.; Hallquist, M.; Pagels, J. H. Secondary organic aerosol formation from idling gasoline passenger vehicle emissions investigated in a smog chamber. *Atmos. Chem. Phys.* **2013**, *13*, 6101−6116.

(24) Liu, T.; Wang, X.; Deng, W.; Hu, Q.; Ding, X.; Zhang, Y.; He, Q.; Zhang, Z.; Lu, S.; Bi, X.; Chan, J.; Yu, J. Secondary organic aerosol formation from photochemical aging of light-duty gasoline vehicle exhausts in a smog chamber. *Atmos. Chem. Phys.* **2015**, *15*, 9049−9062.

(25) Karavalakis, G.; Short, D.; Vu, D.; Russell, R.; Hajbabaei, M.; Asa-Awuku, A.; Durbin, T. D. Evaluating the effects of aromatics content in gasoline on gaseous and particulate matter emissions from SI-PFI and SI-DI vehicles. *Environ. Sci. Technol.* **2015**, *49*, 7021−7031.

(26) Chen, L.; Liang, Z.; Zhang, X.; Shuai, S. Characterizing particulate matter emissions from GDI and PFI vehicles under transient and cold start conditions. *Fuel* **2017**, *189*, 131−140.

(27) Stevens, E.; Steeper, R. Piston wetting in an optical DISI engine: Fuel films, pool fires, and soot generation. *SAE Tech. Pap. Ser.* **2001**, 2001−01−1203.

(28) Karlsson, R. B.; Heywood, J. B. Piston fuel film observations in an optical access GDI engine. *SAE Tech. Pap. Ser.* **2001**, 2001−01−2022.

(29) Piock, W.; Hoffmann, G.; Berndorfer, A.; Salemi, P.; Fusshoeller, B. Strategies towards meeting future particulate matter emission requirements in homogeneous gasoline direct injection engines. *SAE Int. J. Engines* **2011**, *4*, 1455−1468.

(30) Yang, J.; Roth, P.; Durbin, T. D.; Johnson, K. C.; Cocker, D. R., III; Asa-Awuku, A.; Brezny, R.; Geller, M.; Karavalakis, G. Gasoline particulate filters as an effective tool to reduce particulate and PAH emissions from GDI vehicles: A case study with two GDI vehicles. *Environ. Sci. Technol.* **2018**, *52*, 3275−3284.

(31) Mamakos, A.; Martini, G.; Marotta, A.; Manfredi, U. Assessment of different technical options in reducing particle emissions from gasoline direct injection vehicles. *J. Aerosol Sci.* **2013**, *63*, 115−125.

(32) Chan, T. W.; Meloche, E.; Kubsh, J.; Brezny, R. Black carbon emissions in gasoline exhaust and a reduction alternative with a gasoline particulate filter. *Environ. Sci. Technol.* **2014**, *48*, 6027−6034.

(33) Du, Z.; Hu, M.; Peng, J.; Zhang, W.; Zheng, J.; Gu, F.; Qin, Y.; Yang, Y.; Li, M.; Wu, Y.; Shao, M.; Shuai, S. Comparison of primary aerosol emission and secondary aerosol formation from gasoline direct injection and port fuel injection vehicles. *Atmos. Chem. Phys.* **2018**, *18*, 9011−9023.

(34) Zhao, Y.; Lamber, A. T.; Saleh, R.; Saliba, G.; Robinson, A. L. Secondary organic aerosol production from gasoline vehicle exhaust: Effects of engine technology, cold start, and emission certification standard. *Environ. Sci. Technol.* **2018**, *52*, 1253−1261.

(35) Karjalainen, P.; Timonen, H.; Saukko, E.; Kuuluvainen, H.; Saarikoski, S.; Aakko-Saksa, P.; Murtonen, T.; Dal Maso, M.; Ahlberg, E.; Svenningsson, B.; Brune, W. H.; Hillamo, R.; Keskinen, J.; Rönkkö, T. Time-resolved characterization of primary and secondary particle emissions of a modern gasoline passenger car. *Atmos. Chem. Phys.* **2016**, *16*, 8559−8470.

(36) Pieber, S. M.; Kumar, N. K.; Klein, F.; Comte, P.; Bhattu, D.; Dommen, J.; Bruns, E. A.; Kilic, D.; El Haddad, I.; Keller, A.; Czerwinski, J.; Heeb, N.; Baltensperger, U.; Slowik, J. G.; Prévôt, A. S. H. Gas phase composition and secondary organic aerosol formation from gasoline direct injection vehicles investigated in batch and flow reactors: effects of prototype gasoline particle filters. *Atmos. Chem. Phys.* **2018**, *18*, 9929−9954.

(37) Vu, D.; Roth, P.; Berte, T.; Yang, J.; Cocker, D.; Durbin, T.; Karavalakis, G.; Asa-Awuku, A. Using a new Mobile Atmospheric Chamber (MACh) to investigate the formation of secondary aerosols from mobile sources: The case of gasoline direct injection vehicles. *J. Aerosol Sci.*, manuscript under review.

(38) Aiken, A. C.; DeCarlo, P. F.; Kroll, J. H.; Worsnop, D. R.; Huffman, J. A.; Docherty, K. S.; Ulbrich, I. M.; Mohr, C.; Kimmel, J. R.; Sueper, D.; Sun, Y.; Zhang, Q.; Trimborn, A.; Northway, M.; Ziemann, P. J.; Canagaratna, M. R.; Onasch, T. B.; Alfarra, M. R.; Prevot, A. S. H.; Dommen, J.; Duplissy, J.; Metzger, A.; Baltensperger, U.; Jimenez, J. L. O/C and OM/OC ratios of primary, secondary, and ambient organic aerosols with high-resolution time-of-flight aerosol mass spectrometry. *Environ. Sci. Technol.* **2008**, *42*, 4478−4485.

(39) DeCarlo, P. F.; Kimmel, J. R.; Trimborn, A.; Northway, M. J.; Jayne, J. T.; Aiken, A. C.; Gonin, M.; Fuhrer, K.; Horvath, T.; Docherty, K. S.; Worsnop, D. R.; Jimenez, J. L. Field-Deployable, High-Resolution, Time-of-Flight Aerosol Mass Spectrometer. *Anal. Chem.* **2006**, *78*, 8281−8289.

(40) Villani, P.; Picard, D.; Michaud, V.; Laj, P.; Wiedensohler, A. Design and validation of a Volatility Hygroscopic Tandem Differential Mobility Analyzer (VH_TDMA) to characterize the relationships between the thermal and hygroscopic properties of atmospheric aerosol particles. *Aerosol Sci. Technol.* **2008**, *42*, 729−741.

(41) Malloy, Q.; Nakao, S.; Qi, L.; Austin, R. L.; Stothers, C.; Hagino, H.; Cocker, D. R. Real-Time Aerosol Density Determination Utilizing a Modified Scanning Mobility Particle Sizer-Aerosol Particle Mass Analyzer system. *Aerosol Sci. Technol.* **2009**, *43*, 673−678.

(42) Cocker, D. R.; Flagan, R. C.; Seinfeld, J. H. State-of-the-art chamber facility for studying atmospheric aerosol chemistry. *Environ. Sci. Technol.* **2001**, *35*, 2594−2601.

(43) Maricq, M. M.; Szente, J. J.; Jahr, K. The impact of ethanol fuel blends on PM emissions from a light-duty GDI vehicle. *Aerosol Sci. Technol.* **2012**, *46*, 576−583.

(44) Yang, J.; Roth, P.; Ruehl, C. R.; Shafer, M. M.; Antkiewicz, D. S.; Durbin, T. D.; Cocker, D.; Asa-Awuku, A.; Karavalakis, G. Physical, chemical, and toxicological characteristics of particulate emission from current technology gasoline direct injection vehicles. *Sci. Total Environ.* **2019**, *650*, 1182−1194.

(45) Nakao, S.; Shrivastava, M.; Nguyen, A.; Cocker, D., III Interpretation of secondary organic aerosol formation from diesel exhaust photooxidation in an environmental chamber. *Aerosol Sci. Technol.* **2011**, *45*, 964−972.

(46) Squizzato, S.; Masiol, M.; Brunelli, A.; Pistollato, S.; Tarabotti, E.; Rampazzo, G.; Pavoni, B. Factors determining the formation of secondary inorganic aerosol: a case study in the Po Valley (Italy). *Atmos. Chem. Phys.* **2013**, *13*, 1927−1939.

(47) Kroll, J. H.; Seinfeld, J. H. Chemistry of secondary organic aerosol: Formation and evolution of low-volatility organics in the atmosphere. *Atmos. Environ.* **2008**, *42*, 3593−3624.

(48) Gong, J.; Rutland, C. Three way catalyst modeling with ammonia and nitrous oxide kinetics for a lean burn spark ignition direct injection (SIDI) gasoline engine. *SAE Tech. Pap. Ser.* **2013**, 2013−01−1572.

(49) Heeb, N. V.; Forss, A. M.; Bruhlmann, S.; Luscher, R.; Saxer, C. J.; Hug, P. Three-way catalyst-induced formation of ammonia-velocity and acceleration-dependent emission factors. *Atmos. Environ.* **2006**, *40*, 5986−5997.

(50) Presto, A. A.; Gordon, T. D.; Robinson, A. L. Primary to secondary organic aerosol: evolution of organic emissions from mobile combustion sources. *Atmos. Chem. Phys.* **2014**, *14*, 5015−5036.

(51) Ng, N. L.; Canagaratna, M. R.; Zhang, Q.; Jimenez, J. L.; Tian, J.; Ulbrich, I. M.; Kroll, J. H.; Docherty, K. S.; Chhabra, P. S.; Bahreini, R.; Murphy, S. M.; Seinfeld, J. H.; Hildebrandt, L.; Donahue, N. M.; DeCarlo, P. F.; Lanz, V. A.; Prévôt, A. S. H.; Dinar, E.; Rudich, Y.; Worsnop, D. R. Organic aerosol components observed in Northern Hemispheric datasets from Aerosol Mass Spectrometry. *Atmos. Chem. Phys.* **2010**, *10*, 4625−4641.

(52) Heald, C. L.; Kroll, J. H.; Jimenez, J. L.; Cocherty, K. S.; DeCarlo, P. F.; Aiken, A. C.; Chen, Q.; Martin, S. T.; Farmer, D. K.; Artaxo, P. A simplified description of the evolution of organic aerosol composition in the atmosphere. *Geophys. Res. Lett.* **2010**, *37*, L08803.

(53) Chan, A. W. H.; Kautzman, K. E.; Chhabra, P. S.; Surratt, J. D.; Chan, M. N.; Crounse, J. D.; Kurten, A.; Wennberg, P. O.; Flagan, R. C.; Seinfeld, J. H. Secondary organic aerosol formation from photooxidation of naphthalene and alkylnaphthalenes: implications for oxidation of intermediate volatility organic compounds (IVOCs). *Atmos. Chem. Phys.* **2009**, *9*, 3049−3060.

(54) Peng, J.; Hu, M.; Du, Z.; Wang, Y.; Zheng, J.; Zhang, W.; Yang, Y.; Qin, Y.; Zheng, R.; Xiao, Y.; Wu, Y.; Lu, S.; Wu, Z.; Guo, S.; Mao, H.; Shuai, S. Gasoline aromatics: a critical determinant of urban secondary organic aerosol formation. *Atmos. Chem. Phys.* **2017**, *17*, 10743−10752.